PHYSICAL REVIEW B **68**, 100101(R) (2003)

# *Ab initio* predicted metastable TlI-like phase in the $B1$ to $B2$ high-pressure transition of CaO

Michele Catti*
*Dipartimento di Scienza dei Materiali, Università di Milano Bicocca, via Cozzi 53, 20125 Milano, Italy*
(Received 2 July 2003; published 5 September 2003)

Three different pathways have been analyzed, by periodic DFT-GGA-LCAO calculations, for the rocksalt-($B1$) to CsCl-type ($B2$) phase transformation of calcium oxide at the equilibrium pressure of 64.7 GPa. The monoclinic $P2_1/m$ mechanism shows a lower enthalpy barrier (0.13 eV) with respect to the other ones ($R\bar{3}m$ and $Pmmn$), and a secondary minimum in its enthalpy profile gives evidence of a metastable intermediate phase with TlI-like structure and coordination number 7 for both Ca and O. The changes of chemical bonding along the transition path are analyzed.

DOI: 10.1103/PhysRevB.68.100101 PACS number(s): 61.50.Ah, 61.50.Ks, 62.50.+p, 64.70.Kb

The atomic-scale mechanisms of structural phase transitions are a challenging issue of solid-state science, as their understanding may give access to the kinetics of such processes. However, experimental investigations by direct probes are difficult, because nonequilibrium states are usually involved. This holds particularly for reconstructive transformations, where primary chemical bonds are broken and the space-group symmetries of the two solid phases are unrelated.[1] In such cases, quantum-mechanical calculations of least free energy pathways in the appropriate configurational space can be a powerful tool to address the problem. For pressure-dependent phase transitions at $T=0$ K, the relevant free energy function is enthalpy $H=E+pV$, to be obtained from the quantum-mechanical ground-state total energy $E$. Lattice periodicity is assumed to be preserved during the transition, and activation enthalpy barriers can be computed and compared for different mechanisms, in order to detect the one most favored energetically.

Although, in principle, a brute force method could be employed in the most general reaction coordinate space, neglecting any symmetry information, in practice a particular subspace is usually chosen, characterized by a symmetry which is a common subgroup of both space groups of the end phases. This choice can be made by guesses, as in the cases of the $B3$ to $B1$ (SiC and ZnS) (Ref. 2) and $B4$ to $B1$ (GaN) (Ref. 3) transitions, or by a full group-theoretical analysis (cf. the $B1/B2$ transition of NaCl).[4] In any case, the transformation pathway can be of two kinds. In type I, the process is driven by a pure lattice distortion, which can be taken as order parameter, so that all atoms occupy the same sites before and after the transition; the site symmetries, however, are expected to change. The fractional atomic coordinates in the low-symmetry reference frame are the same for both end phases, but they may change in the intermediate states. In type II, on the other hand, a net atomic motion within the unit cell occurs along the transformation, in addition to the lattice distortion, so that the fractional coordinates of some atoms are different in the two end phases. This is the case of both mechanisms considered for the $B3$ to $B1$ transition.[2]

The phase transformation from the NaCl-type ($Fm\bar{3}m$ space group, $Z=4$ formula units per unit cell, $B1$ phase) to the denser CsCl-type structure ($Pm\bar{3}m$, $Z=1$, $B2$ phase) is a typical reconstructive process, and occurs at high pressure for a number of alkali halides (NaCl, KCl, RbCl, NaBr) and alkaline-earth oxides (CaO, SrO, BaO). The transition pressures $p_t$ are, for instance, 27 GPa for NaCl and 60 GPa for CaO (cf. Refs. 5 and 6). Three main mechanisms have been proposed for the $B1$ to $B2$ transition of NaCl and other halides. The first two are the classical Buerger[1] and Watanabe, Tokonami, and Morimoto (WTM)[7] pathways, based on $R\bar{3}m$ rhombohedral and $Pmmn$ orthorhombic intermediate states, respectively, and they were suggested on the basis of x-ray diffraction results on the relative crystallographic orientation of the low-($B1$) and high-($B2$) pressure phases. Theoretical calculations were performed on the first one[8] and on both.[9] The third mechanism was recently proposed by Stokes and Hatch[4] on group-theoretical grounds, and relies upon a $P2_1/m$ monoclinic intermediate state. This pathway was shown to be related to an unstable phonon of the $R\bar{3}m$ structure at the $F$ point in the first Brillouin zone.[4]

The first aim of this work was to compute accurate enthalpy profiles vs the transformation coordinates at the transition pressure $p_t$ for each of the three main pathways $R\bar{3}m$ (Buerger), $Pmmn$ (Watanabe *et al.*) and $P2_1/m$ [Stokes and Hatch (SH)], in the cases of NaCl and CaO, in order to definitely assess the corresponding activation enthalpy values and then find the most favored mechanism. The second aim was to analyze the new monoclinic mechanism in detail, so as to enlighten the chemical bonding evolution underlying it. Unexpectedly, clear evidences of an intermediate metastable phase were obtained for the latter pathway, which also showed the lowest enthalpy barrier. Here the first most interesting results, concerning CaO, are reported.

In Table I, each transition path is characterized vertically by a set of three transformation matrices: the first two express the unit-cell vectors of the $B1$ and $B2$ structures as linear combinations of those of the intermediate state, and the third one relates directly the $B2$ to the $B1$ lattice; the coefficients are given as columns of the matrices. Then the atomic fractional coordinates of Ca and O referred to the unit cell of the intermediate state are reported. In the $R\bar{3}m$ case, all coordinates are fixed by symmetry throughout the transformation; in $P2_1/m$, $x$ and $z$ can be relaxed in the intermediate states, but they take on the same fixed values (given in parentheses in Table I) in the $B1$ and $B2$ end phases. Therefore, according to the above classification both transforma-

 

TABLE I. For each of the three pathways between the $B1$ ($Fm\bar{3}m$) and $B2$ ($Pm\bar{3}m$) structures of CaO, the transformation matrices relating the unit cells of both end phases to that of the intermediate state (IS), and those of the end phases to each other, are given vertically. The atomic fractional coordinates in the IS unit cell are also included. $a_I$ and $a_{II}$ are the cubic cell edges of the $B1$ and $B2$ phases, respectively.

| $R\bar{3}m$ ($Z=1$) | $P2_1/m$ ($Z=2$) | $Pmmn$ ($Z=2$) |
|---|---|---|
| $R\bar{3}m \rightarrow Fm\bar{3}m$ | $P2_1/m \rightarrow Fm\bar{3}m$ | $Pmmn \rightarrow Fm\bar{3}m$ |
| $\begin{bmatrix} -1 & 1 & 1 \\ 1 & -1 & 1 \\ 1 & 1 & -1 \end{bmatrix}$ | $\begin{bmatrix} 0 & 0 & 1 \\ 1 & -1 & 0 \\ 1 & 1 & -1 \end{bmatrix}$ | $\begin{bmatrix} 1 & 0 & 0 \\ 0 & 1 & -1 \\ 0 & 1 & 1 \end{bmatrix}$ |
| $R\bar{3}m \rightarrow Pm\bar{3}m$ | $P2_1/m \rightarrow Pm\bar{3}m$ | $Pmmn \rightarrow Pm\bar{3}m$ |
| $\begin{bmatrix} 1 & 0 & 0 \\ 0 & 1 & 0 \\ 0 & 0 & 1 \end{bmatrix}$ | $\begin{bmatrix} \frac{1}{2} & \frac{1}{2} & 0 \\ -\frac{1}{2} & \frac{1}{2} & 0 \\ 0 & 0 & 1 \end{bmatrix}$ | $\begin{bmatrix} \frac{1}{2} & 0 & \frac{1}{2} \\ \frac{1}{2} & 0 & -\frac{1}{2} \\ 0 & 1 & 0 \end{bmatrix}$ |
| $Fm\bar{3}m \rightarrow Pm\bar{3}m$ | $Fm\bar{3}m \rightarrow Pm\bar{3}m$ | $Fm\bar{3}m \rightarrow Pm\bar{3}m$ |
| $\begin{bmatrix} 0 & \frac{1}{2} & \frac{1}{2} \\ \frac{1}{2} & 0 & \frac{1}{2} \\ \frac{1}{2} & \frac{1}{2} & 0 \end{bmatrix}$ | $\begin{bmatrix} 0 & \frac{1}{2} & \frac{1}{2} \\ \frac{1}{2} & 0 & \frac{1}{2} \\ \frac{1}{2} & \frac{1}{2} & 0 \end{bmatrix}$ | $\begin{bmatrix} \frac{1}{2} & 0 & \frac{1}{2} \\ \frac{1}{4} & \frac{1}{2} & -\frac{1}{4} \\ -\frac{1}{4} & \frac{1}{2} & \frac{1}{4} \end{bmatrix}$ |
| Ca: 0, 0, 0 | $x_1\ (\frac{1}{4})$, $\frac{1}{4}$, $z_1(0)$ | $\frac{1}{4}$, $\frac{1}{4}$, $z\ (\frac{1}{4} \rightarrow \frac{1}{2})$ |
| O: $\frac{1}{2}$, $\frac{1}{2}$, $\frac{1}{2}$ | $x_2\ (\frac{3}{4})$, $\frac{1}{4}$, $z_2(\frac{1}{2})$ | $\frac{1}{4}$, $\frac{3}{4}$, $z+\frac{1}{2}\ (\frac{3}{4} \rightarrow 1)$ |
| $B1$ phase | | |
| $a=a_I/\sqrt{2}$ | $a=a_I\sqrt{\frac{3}{2}}$ | $a=a_I$ |
| $\alpha=60°$ | $b=c=a_I/\sqrt{2}$ | $b=c=a_I/\sqrt{2}$ |
| | $\beta=54.74°$ | $z=\frac{1}{4}$ |
| $B2$ phase | | |
| $a=a_{II}$ | $a=b=a_{II}\sqrt{2}$ | $a=b=a_{II}\sqrt{2}$ |
| $\alpha=90°$ | $c=a_{II}$ | $c=a_{II}$ |
| | $\beta=90°$ | $z=\frac{1}{2}$ |
| Order parameter | | |
| $\alpha$ | $\beta$ | $z$ |

tion mechanisms belong to type I. On the other hand, for the $Pmmn$ mechanism the $z$ coordinate of one of the two atoms is a free parameter in the intermediate states, varying between different end values that correspond to the $B1$ and $B2$ structures. In this case the mechanism is thus of type II. Accordingly, a unit-cell angle ($\alpha$ for rhombohedral $R\bar{3}m$ and $\beta$ for monoclinic $P2_1/m$) was chosen as transformation coordinate (order parameter) of the first two mechanisms and the $z$(Ca) atomic fractional coordinate for the $Pmmn$ pathway (Table I).

The total energy of each configuration was obtained by *ab initio* calculations employing localized basis functions (atomic orbitals), and a DFT-GGA-PBE Hamiltonian [CRYSTAL98 code (Ref. 10)]. The generalized gradient approximation, implemented in this case through the Perdew-Burke-Ernzerhof scheme,[11] provides a nonlocal exchange-correlation potential which usually works better than that of

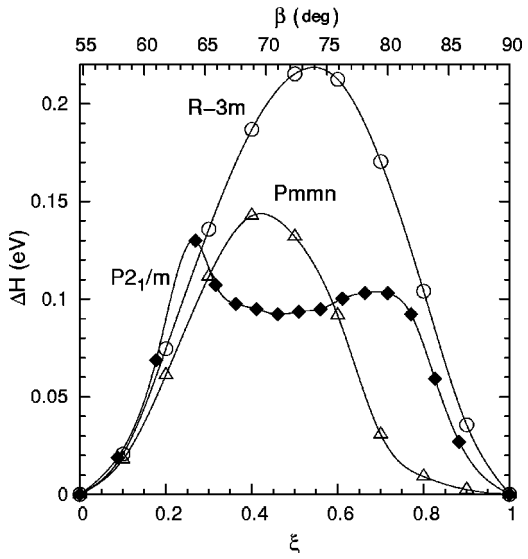


FIG. 1. Enthalpy of the intermediate states of CaO vs the normalized transformation coordinate $\xi$, calculated along three different pathways of the $B1$ ($\xi=0$) to $B2$ ($\xi=1$) phase transition at the equilibrium pressure of 64.7 GPa. The monoclinic $\beta$ angle (upper horizontal axis) refers to the $P2_1/m$ curve only.

local density approximation for simulating transition pressures.[2] An all-electron basis set, based on 22 (Ca) and 18 (O) atomic orbitals, was employed. The radial factors are expressed as linear combinations of Gaussian-type functions of the electron-nucleus distance, according to $8(s)6511(sp)3(d)$G and $8(s)411(sp)1(d)$G contractions for calcium and oxygen, respectively. Coefficients and exponents of the Gaussian functions were taken from Ref. 12. The tolerance for neglect of integrals was set to $10^{-8}$, a Monkhorst grid of $8\times8\times8$ in the first Brillouin zone was used, and the SCF convergence threshold was set to $10^{-8}$ hartree. For each structural configuration, the enthalpy $H$ was minimized at constant pressure with respect to all structural parameters not fixed by space-group symmetry, using a conjugate-gradients routine (LoptCG, courtesy of C. Zicovich-Wilson) based on numerical gradients.

By parabolic fitting of eight $H$ values computed in the range 0–80 GPa for each of the $B1$ and $B2$ phases of CaO, the following curve was obtained: $\Delta H_t(p)=H_{B2}(p)-H_{B1}(p)=0.94456-0.01636p+2.768\times10^{-5}p^2$, with $p$/GPa and $H$/eV. A predicted $p_t$ equilibrium pressure of 64.7 GPa is given by the condition $\Delta H_t(p)=0$. This value compares favorably with the experimental result of 60 GPa.[6] For each of the three pathways presented above, the quantity $\Delta H=H-H_{B1}$ was calculated at constant equilibrium pressure (64.7 GPa) as a function of the transformation coordinate. We define a normalized general transformation coordinate $\xi$, which, for instance, in the $R\bar{3}m$ case is equal to $(\alpha-\alpha_{B1})/(\alpha_{B2}-\alpha_{B1})$, and similarly for the other paths; then $\xi(B1)=0$ and $\xi(B2)=1$ in all cases. Thus we are able to report the enthalpy profiles obtained for the three pathways on the same scale as $\Delta H(\xi)$ in Fig. 1. As a first remark, the Buerger mechanism can be definitely ruled out with respect to the other two, because of its much higher enthalpy barrier

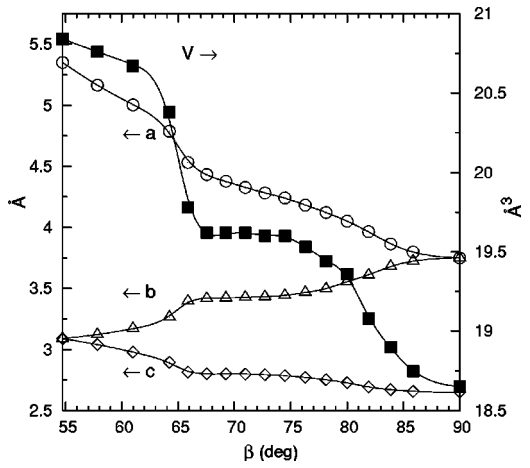


FIG. 2. Unit-cell edges (left axis) and volume (right axis) of CaO along the $P2_1/m$ path of the $B1$ to $B2$ transition vs the monoclinic $\beta$ angle taken as transformation coordinate at $p=64.7$ GPa.

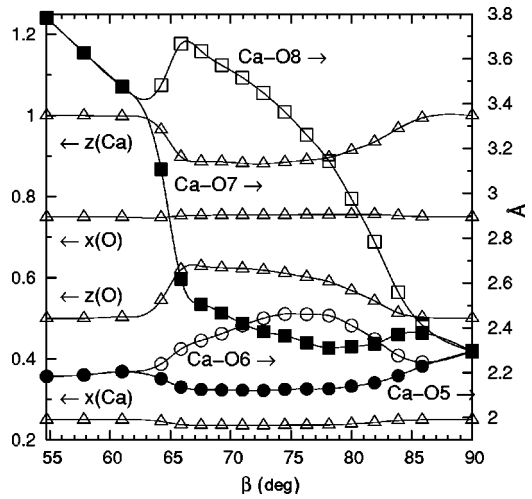


FIG. 3. Symmetry-unconstrained atomic fractional coordinates (triangles, left axis), and some Ca-O interatomic distances (circles and squares, right axis) of the $P2_1/m$ intermediate states plotted against the $B1$ to $B2$ transformation coordinate (monoclinic $\beta$ angle).

of 0.215 eV compared to 0.143 eV (WTM) and 0.130 eV (SH). This result is important, as until recently the enthalpic preference between the $R\bar{3}m$ and $Pmmn$ pathways for the NaCl case was debated (cf. e.g., Refs. 4 and 9). As second point, the $P2_1/m$ mechanism appears to be slightly favored over the $Pmmn$ one, with an activation enthalpy lower by 0.013 eV. At sufficiently high temperature, the hierarchy of free energy barriers of the latter two pathways might be affected by the entropic term with its phonon contributions, but this should certainly not concern the $R\bar{3}m$ mechanism, in view of its much larger enthalpic term. In future work, calculations of enthalpy profiles for all three pathways will be extended also to pressures higher and lower than $p_t$.

Indeed, the most striking feature appearing in Fig. 1 is the unusual shape of the $\Delta H$ curve for the monoclinic pathway. In particular, a broad intermediate minimum appears at $\beta=71°$ (with $\Delta H=0.093$ eV), indicating the presence of a well-defined metastable phase along the transformation path, whose structure is characterized by $a=4.327$, $b=3.428$, $c=2.799$ Å, $x(\mathrm{Ca})=0.2359$, $z(\mathrm{Ca})=0.8824$, $x(\mathrm{O})=0.7547$, $z(\mathrm{O})=0.6228$. The formation of the metastable phase can be detected, too, by looking at the monoclinic lattice constants plotted vs the order parameter $\beta$ (Fig. 2). A sharp jump at around $\beta=65°$ is shown particularly by the unit-cell volume, corresponding to the onset of the enthalpy well in Fig. 1. Then a flat region follows, concluded by a smoother jump in the final $\beta$ range. A similar behavior is shown by the unit-cell edges, and also by the $x$ and $z$ atomic fractional coordinates of Ca and O (Fig. 3). Such results can be explained by an atomistic analysis of the $P2_1/m$ mechanism, also with reference to the Buerger pathway $R\bar{3}m$.

In Fig. 4 (left) the $B1$ structure of CaO in the monoclinic reference frame is shown, including the outline of the primitive cubic cell (rhombohedron with $\alpha=60°$). In the $R\bar{3}m$ $B1/B2$ mechanism, the rhombohedron is squeezed along its threefold axis with an increase of the six equal Ca-O bond lengths, and a decrease of the two equal nonbonded Ca-O distances, till all eight contacts have the same length. Thus, the coordination number (CN) of Ca (and O) evolves continuously from 6 to 8 according to the $6+2$ scheme. In the $P2_1/m$ mechanism, on the other hand, the rhombohedron is compressed along the long diagonal of one of its faces. The symmetry lowering transforms the $6+2$ Ca-O distances into $4+2+2$, if the atomic fractional coordinates do not relax from their original values, but into $2+2+1+1+1+1$, when relaxation occurs (cf. Fig. 3 for $\beta\geqslant 64°$). In particular, in the last case the long Ca-O7 and Ca-O8 contacts may take different lengths, and this opens the way to structural states with CN=7 intermediate between 6 ($B1$) and 8 ($B2$). This

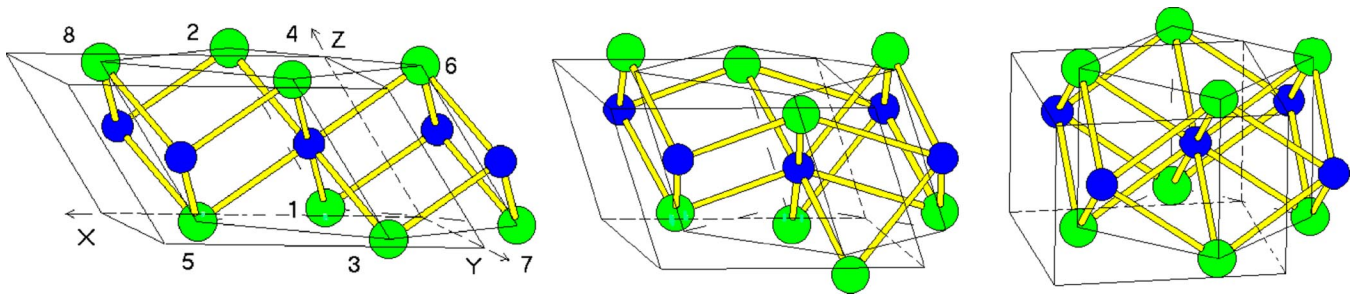


FIG. 4. (Color online) Crystal structure of the CaO monoclinic metastable state with $\beta=71.0°$ (middle), similar to the TlI structure, along the $P2_1/m$ pathway connecting the $B1$ (left) and $B2$ (right) phases. Oxygen atoms are numbered.

is what indeed happens for all intermediate states with $\beta$ between 66° and 80° (Fig. 4, middle), where the Ca-O6 and Ca-O7 bonds range from 2.33 to 2.41 Å and from 2.56 to 2.32 Å, respectively, thus attaining a more or less distorted sevenfold first coordination sphere for both Ca and O (Fig. 3). On the other hand, the $Pmmn$ mechanism behaves in this respect as the Buerger one, because its scheme of first-neighbors chemical bonds is $2+2+2+2$, so that two symmetrical bonds lengthen and two shorten in the continuous passage from CN 6 to 8, with no possibility of attaining a sevenfold intermediate coordination. We conclude therefore that the particular stability of this structure based on CN $=7$ is the main reason favoring the $P2_1/m$ mechanism with respect to the other two.

A closer examination of the sevenfold coordinate intermediate structure revealed its similarity to that of the stable phases of alkali hydroxides, like KOH and RbOH (monoclinic $P2_1/m$), and to the orthorhombic $Cmcm$ structure of the yellow form of TlI.[13] In particular, the latter one ($a=4.57$, $b=12.92$, $c=5.24$ Å; Tl: 0, 0.11, 1/4; I: 0, 0.37, 1/4) can be obtained from the $P2_1/m$ lattice by the transformation $[001/20-1/010]$, with the constrain that $\cos\beta=c/2a$, and $z=-x/2$ for the monoclinic atomic coordinates. The $P2_1/m$ intermediate state of CaO closest to the TlI structure occurs at $\beta=71°$, corresponding to the minimum of the enthalpy well in Fig. 1. Therefore, the metastable phase of CaO can be interpreted as a slightly distorted monoclinic version of the TlI structure-type. Indeed, it is interesting to remark that AgCl was found experimentally to undergo at high pressure a series of phase transitions from the $B1$ structure to a TlI-type orthorhombic phase, a KOH-type monoclinic phase, and eventually to the $B2$ structure.[14] Also for NaBr and NaI, a high-pressure transformation from the $B1$ to the TlI-like phase was recently reported from x-ray diffraction results.[15] In the case of CaO, the TlI-like phase does not show a thermodynamic stability range of its own: we computed the enthalpy of TlI-like $Cmcm$-CaO vs pressure, and found that it may be lower than either the $B2$ ($p<50$ GPa) or $B1$ ($p>80$ GPa) phases, but it is never smaller than both of them at the same pressure. Thus, the distorted TlI-like phase appears only metastably along the transformation path of CaO from $B1$ to $B2$. Further work is planned to investigate its role in the $B1$ to $B2$ transitions of other systems.

*Email address: catti@mater.unimib.it

[1] M. Buerger, in *Phase Transformations in Solids*, edited by R. Smoluchowski, J.E. Mayers, and W.A. Weyl (Wiley, New York, 1948), pp. 183–211.

[2] M. Catti, Phys. Rev. Lett. **87**, 035504 (2001); M. Catti, Phys. Rev. B **65**, 224115 (2002); J.M. Perez-Mato *et al.*, Phys. Rev. Lett. **90**, 049603 (2003); M. Catti, *ibid.* **90**, 049604 (2003).

[3] S. Limpijumnong and W.R.L. Lambrecht, Phys. Rev. Lett. **86**, 91 (2001).

[4] H.T. Stokes and D.M. Hatch, Phys. Rev. B **65**, 144114 (2002).

[5] S. Froyen and M.L. Cohen, J. Phys. C **19**, 2623 (1986).

[6] P. Richet, H.K. Mao, and P.M. Bell, J. Geophys. Res. **93**, 15279 (1986).

[7] M. Watanabe, M. Tokonami, and N. Morimoto, Acta Crystallogr., Sect. A: Cryst. Phys., Diffr., Theor. Gen. Crystallogr. **A33**, 284 (1977).

[8] A. Martín-Pendás, V. Luaña, J.M. Recio, M. Florez, E. Francisco, M.A. Blanco, and L.N. Kantorovich, Phys. Rev. B **49**, 3066 (1994).

[9] C.E. Sims, G.D. Barrera, N.L. Allan, and W.C. Mackrodt, Phys. Rev. B **57**, 11164 (1998).

[10] V.R. Saunders *et al.*, *CRYSTAL98: User's Manual* (University of Torino, Italy/CLRC Daresbury Laboratory, United Kingdom, 1999).

[11] J.P. Perdew, K. Burke, and M. Ernzerhof, Phys. Rev. Lett. **77**, 3865 (1996).

[12] M.P. Habas, R. Dovesi, and A. Lichanot, J. Phys.: Condens. Matter **10**, 6897 (1998).

[13] A.F. Wells, *Structural Inorganic Chemistry* (Clarendon, Oxford, 1975).

[14] K. Kusaba, Y. Syono, T. Kikegawa, and O. Shimomura, J. Phys. Chem. Solids **56**, 751 (1995).

[15] J.M. Léger *et al.*, J. Phys.: Condens. Matter **10**, 4201 (1998).